Tailored Single-Atom Collisions at Ultralow Energies

Felix Schmidt,[1] Daniel Mayer,[1] Quentin Bouton,[1] Daniel Adam,[1] Tobias Lausch,[1]
Jens Nettersheim,[1] Eberhard Tiemann,[2] and Artur Widera[1,3,*]

[1]*Department of Physics and Research Center OPTIMAS, Technische Universität Kaiserslautern, 67663 Kaiserslautern, Germany*
[2]*Institut für Quantenoptik, Leibniz Universität Hannover, 30167 Hannover, Germany*
[3]*Graduate School Materials Science in Mainz, Gottlieb-Daimler-Strasse 47, 67663 Kaiserslautern, Germany*

(Received 22 October 2018; published 8 January 2019)

We employ collisions of individual atomic cesium (Cs) impurities with an ultracold rubidium (Rb) gas to probe atomic interaction with hyperfine- and Zeeman-state sensitivity. Controlling the Rb bath's internal state yields access to novel phenomena observed in interatomic spin exchange. These can be tailored at ultralow energies, owing to the excellent experimental control over all relevant energy scales. First, detecting spin-exchange dynamics in the Cs hyperfine-state manifold, we resolve a series of previously unreported Feshbach resonances at magnetic fields below 300 mG, separated by energies as low as $h \times 15$ kHz. The series originates from a coupling to molecular states with binding energies below $h \times 1$ kHz and wave function extensions in the micrometer range. Second, at magnetic fields below $\approx$100 mG, we observe the emergence of a new reaction path for alkali atoms, where in a single, direct collision between two atoms two quanta of angular momentum can be transferred. This path originates from the hyperfine analog of dipolar spin-spin relaxation. Our work yields control of subtle ultralow-energy features of atomic collision dynamics, opening new routes for advanced state-to-state chemistry, for controlling spin exchange in quantum many-body systems for solid-state simulations, or for determination of high-precision molecular potentials.

DOI: 10.1103/PhysRevLett.122.013401

Understanding and controlling collisions of two atoms at ultralow energies are the basis of quantum engineering [1,2], chemistry [3,4], and metrology [5] applications. Advances in cooling and trapping of atoms have opened experimental routes to study atomic interactions with well-defined quantum states at ultracold temperatures [6]. The energy scale and resolution of individual collision and reaction processes are set by the thermal broadening in a finite-temperature system, as well as the system's lifetime. Collisional spectroscopy involving single ions [7–9] or atoms [10] are capable of tracing individual collision pathways or spin-controlled collisions, with an associated energy resolution in the order of few $h \times$ GHz. Recently, also Rydberg excitations in cold gases yield access to single ion-atom collisions [11,12], where an energy resolution in the $h \times$ MHz regime is achieved for excitation lifetimes of a few microseconds. By contrast, collisional energies for neutral atom mixtures at ultralow temperatures are in the order of few $h \times$ kHz. These low collisional energies have been employed, e.g., to determine scattering phase shifts in an atomic clock [13] or to build ultracold molecules from pairs of atoms in optical lattices [2,14]. Hence, probing the interspecies interaction of individual collisional channels should be possible with unprecedented resolution, where we focus on scattering processes of unbound ultracold atoms in close proximity to the dissociation threshold, rather than bound molecular states [15,16].

Low energies and internal-state resolution yield access to intriguing phenomena of a single atom-atom collision that originate from the complex interplay of collisional, Zeeman, hyperfine, and molecular interaction energies. Particularly, we reveal ultralow-energy features of interspecies spin dynamics, interfacing an ultracold ^{87}Rb bath with single neutral ^{133}Cs atoms [17,18] via s-wave collisions. A hierarchy of rates for different collisional processes is identified, i.e., elastic collisions and spin exchange (SE) in quanta of $1\hbar$ and $2\hbar$, where respective cross sections σ roughly scale as $\sigma_{\mathrm{el}} \approx 10\sigma_1 \approx 10^2\sigma_2$. We adjust both the internal Rb state and the magnetic-field value to address specific regimes of SE. Scattering channels at such small energies couple to the last bound state in the molecular potential. An unusually small binding energy below $h \times 1$ kHz leads to a giant molecular wave function in the micrometer range. Coupling to this state results in a series of Feshbach resonances in different collisional channels, energetically spaced by less than $h \times 15$ kHz $= k_B \times 350$ nK and detected via SE. Moreover, the hyperfine analog of dipole-dipole coupling can drive SE in quanta of $2\hbar$ between Cs and Rb with a measurable contribution of σ_2.

Experimentally, we prepare a dilute, thermal Rb bath of typically $3.0(6) \times 10^3$ atoms at $T_{\mathrm{Rb}} = 450(80)$ nK in a desired hyperfine state and, independently, on average 6 Cs impurities in the absolute energy ground state [see Fig. 1(a); details are given in Refs. [17,18]]. Subsequently,

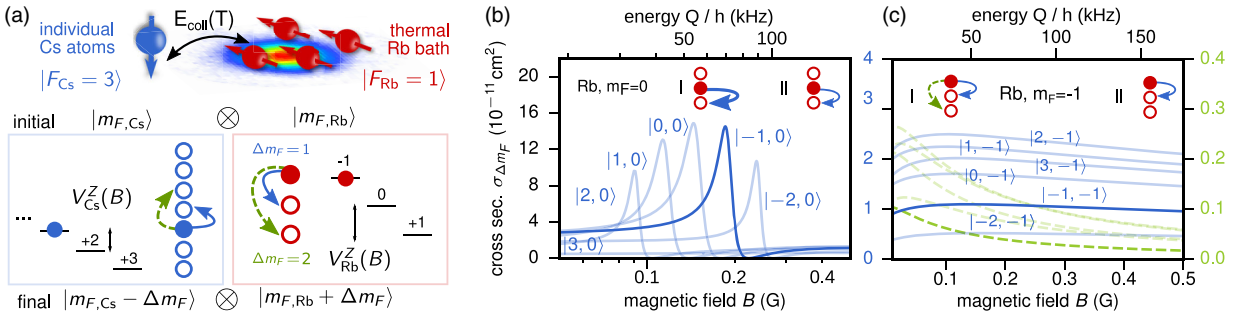

FIG. 1. System overview. (a) In the experiment, individual Cs atoms collide with atoms of an ultracold, thermal Rb bath [temperature typically 450(80) nK, atom number $3.0(6)\times10^3$]. Elastic collisions between Cs and Rb lead to thermalization of Cs in Rb. Additionally, in a spin-exchange (SE) collision, Cs (bottom left) and Rb (bottom right) can exchange angular momentum by $\Delta m_F=1$ (blue, solid) or $\Delta m_F=2$ (green, dashed). Interaction parameters, i.e., collision energy, magnetic field, and internal states, are experimentally controlled, which allows tailoring the dynamics. In a SE collision with $\Delta m_F=1$, the energy $Q=|V^Z_{Rb}-V^Z_{Cs}|=h\times350\ \mathrm{kHz/G}\times B$ is released. (b) Collision cross sections for Rb in $m_{F,Rb}=0$, where only $\Delta m_F=1$ is allowed, showing Feshbach resonances (I) and quasi-constant SE cross sections (II). (c) For Rb in $m_{F,Rb}=-1$, at low B fields $\Delta m_F=+2$ processes become accessible as well (I, dashed lines).

Cs atoms are transported into the Rb bath by means of a species-specific optical potential [19] and SE-driven dynamics of the Cs Zeeman state is studied by measuring the Cs Zeeman population as a function of the interaction duration t_i. By repeating the experiment typically 100 times for constant parameters, information on effective spin dynamics is obtained. In our strongly imbalanced mixture, Cs atoms exclusively interact with Rb atoms in one internal $m_{F,Rb}$ state, and correlations by a second collision with the same Rb atom are negligible, thus realizing particle state control for each collision event. Additionally, the use of only a few Cs atoms is crucial, because it avoids Cs-Cs interaction. In fact, the Cs intraspecies scattering cross section exceeds the interspecies cross section by a factor of ~20, due to a broad negative-field Feshbach resonance [20].

Cs and Rb interact via the Hamiltonian [21]

$$H=E_{\mathrm{coll}}+\sum_{j=\mathrm{Cs,Rb}}(V^Z_j+V^{\mathrm{HFS}}_j)+\hat{H}^{\mathrm{int}}, \qquad (1)$$

with collisional energy E_{coll} and single-particle Zeeman and hyperfine energies V^Z_j and V^{HFS}_j, respectively. Finally, the interaction of both collision partners $\hat{H}^{\mathrm{int}}$ is determined by a molecular potential model, originating from interparticle singlet and triplet potentials [22]. In our experiment, we control *all* parameters that determine the Cs-Rb dynamics, emerging from (1). These are the temperature ($E_{\mathrm{coll}}\propto T$ [23]), the magnetic field B ($V^Z_j\propto B$), and the internal Rb state (V^{HFS}_b, V^Z_b). In the s-wave limit at low collisional energy, the interaction $\hat{H}^{\mathrm{int}}$ can be effectively expressed in terms of asymptotic Cs (Rb) states, given by total angular momentum $\mathbf{F}_{\mathrm{Cs}}$ ($\mathbf{F}_{\mathrm{Rb}}$) with quantum number F_{Cs} (F_{Rb}) and projections $m_{F,\mathrm{Cs}}$ ($m_{F,\mathrm{Rb}}$) as $\hat{H}^{\mathrm{int}}=\sum_{i=0,1,2}c_i(\mathbf{F}_{\mathrm{Cs}}\cdot\mathbf{F}_{\mathrm{Rb}})^i$ (for details, see [23]). We conduct experiments in hyperfine ground states $F_{\mathrm{Cs}}=3$, $F_{\mathrm{Rb}}=1$, and denote collisional channels by $|m_{F,\mathrm{Cs}},m_{F,\mathrm{Rb}}\rangle$. For Cs-Rb distances of few $10a_0$ ($a_0\approx0.5$ Å is the Bohr radius), the interaction energy $\hat{H}^{\mathrm{int}}$ reaches values that are of the order of V^{HFS}_j, coupling $\mathbf{F}_{\mathrm{Cs}}$ and $\mathbf{F}_{\mathrm{Rb}}$ [22]. The coupling can lead to state-changing collisions $|m'_{F,\mathrm{Cs}},m'_{F,\mathrm{Rb}}\rangle=|m_{F,\mathrm{Cs}}-\Delta m_F,m_{F,\mathrm{Rb}}+\Delta m_F\rangle$, and the tensorial structure of $\hat{H}^{\mathrm{int}}$ allows processes with $\Delta m_F=0,\pm1,\pm2$. For $\Delta m_F=0$ processes, the internal states remain unchanged and the collision is elastic, setting the foundation for the description of interacting Bose gases [32] and thermalization, e.g., [33]. SE processes with $\Delta m_F\neq0$ exchange angular momentum between the collision partners [see Fig. 1(a)], which is the basis for spinor dynamics [34]. Energy and angular momentum conservation restrict observable SE processes, as shown in Fig. 1(a). At low magnetic fields B, Zeeman energies $V^Z_j=\mu_j m_{Fj}B$ of Cs and Rb determine the direction of SE due to their different magnetic moments μ_j ($\mu_{\mathrm{Rb}}=2\mu_{\mathrm{Cs}}$). SE processes with $\Delta m_F=1,2$ are exoergic, while SE with $\Delta m_F=-1$, -2 is endoergic and energetically forbidden for magnetic fields used here. Exoergic processes $\Delta m_F=1,2$ are further restricted by angular momentum conservation. For Rb in $m_{F,\mathrm{Rb}}=0$, only $\Delta m_F=1$ is allowed, while for $m_{\mathrm{Rb}}=-1$, both $\Delta m_F=1,2$ processes are accessible. By contrast, for $m_{F,\mathrm{Rb}}=1$, SE with positive Δm_F is forbidden. Thus, the magnetic field B and the choice of the Rb $m_{F,\mathrm{Rb}}$ state grant control over collisional phenomena. Scattering cross sections $\sigma_{\Delta m_F}$ for respective SE processes are calculated in a coupled-channel scattering model and shown in Figs. 1(b) and 1(c). The calculations are based on a Cs-Rb interaction potential model, obtained from more than 30×10^3 spectroscopy lines and Feshbach resonances [22]. For Rb bath atoms prepared in $m_{F,\mathrm{Rb}}=0$ [see Fig. 1(b)], our coupled-channel simulations indicate a regime of constant SE cross

sections (regime *II*, $B > 300$ mG), whereas a series of Feshbach resonances in various collision channels $|m_{F,\mathrm{Cs}}, m_{F,\mathrm{Rb}}\rangle$ emerges at magnetic fields below 300 mG (regime *I*). The series originates from a coupling of the asymptotic state $|m_{F,\mathrm{Cs}}, m_{F,\mathrm{Rb}}\rangle$ to the first molecular bound state below the dissociation threshold, with total angular momentum $F = 2$ and a binding energy as low as $-h \times 490$ Hz at the magnetic field $B = 80$ mG, where the first resonance occurs. At these low binding energies, the molecular wave function is highly delocalized with its mean radius calculated to be approximately $4000a_0 \approx 2$ μm. Note that the resonance also yields an enhanced elastic scattering cross section. For ultracold Cs-Cs collisions, resonances have been found in a similar low-field regime [13,35], which is the result of the large reduced masses in both systems (Rb-Cs and Cs-Cs). These lead to a dense spectrum of bound states below the dissociation threshold, which makes the occurrence of Feshbach resonances probable. For bath atoms prepared in $m_{F,\mathrm{Rb}} = -1$ [see Fig. 1(c)] SE with $\Delta m_F = 2$ arises, showing highest cross sections at magnetic fields $\leq$50 mG. This $\Delta m_F = 2$ SE process is so far unreported for collisions of alkali atoms. In fact, for alkalis, scattering cross sections for dipolar spin relaxation, leading to $2\hbar$ processes in dipolar gases [36], are at least 3 orders of magnitude smaller than of SE [23], thus negligible in our system.

As the elastic cross section σ_0 exceeds SE by a factor of $\sim$10, thermalization of Cs impurities to the Rb temperature is ensured in the presence of exoergic SE (see [23]). This allows modeling the time evolution of an initially prepared Cs atom in state $m_{F,\mathrm{Cs}} = 3$ with population $N_{m_{F,\mathrm{Cs}}}$, driven by SE with Rb. The model bases on a rate equation, where all possible SE processes Δm_F are incorporated (see [23]). The collision rates for elastic and SE processes $\Gamma_{\Delta m_F}$, entering this model, are directly calculated from cross sections $\Gamma_{\Delta m_F} = \sigma\langle|\mathbf{v}_{\mathrm{rel}}|\rangle\langle n\rangle$, with expectation values of relative collision velocities $\langle|\mathbf{v}_{\mathrm{rel}}|\rangle$ of thermalized Cs atoms and the independently obtained Cs-Rb density overlap $\langle n\rangle$ (see [23]).

We first explore SE phenomena for the Rb bath in $m_{F,\mathrm{Rb}} = 0$, starting at the high B-field regime [regime *II* in Fig. 1(b)]. Cs atoms are prepared in the $m_{F,\mathrm{Cs}} = 3$ state initially and SE is resolved temporally for a constant magnetic field of 440 mG [Fig. 2(a)]. In the absence of Feshbach resonances, SE cross sections σ_1 of consecutive $|m_{F,\mathrm{Cs}}, m_{F,\mathrm{Rb}} = 0\rangle$ entrance channels are of similar magnitude. Therefore, Cs atoms are subsequently pumped into the final $m_{F,\mathrm{Cs}} = -3$ state in a chain of SE events. As SE is unidirectional, Cs uniformly samples the full quasi-spin space $m_{F,\mathrm{Cs}}$ and the chain of collision events is encoded in the final $m_{F,\mathrm{Cs}}$ state. Thus, due to the fixed ratio of elastic versus SE events, the $m_{F,\mathrm{Cs}}$ state after the interaction also serves as an elastic-collision counter. Interestingly, since collisional cross section are state dependent, this collision probe has non-Markovian character. The measured time evolution is well reproduced by our model [see Figs. 2(c) and 2(d)].

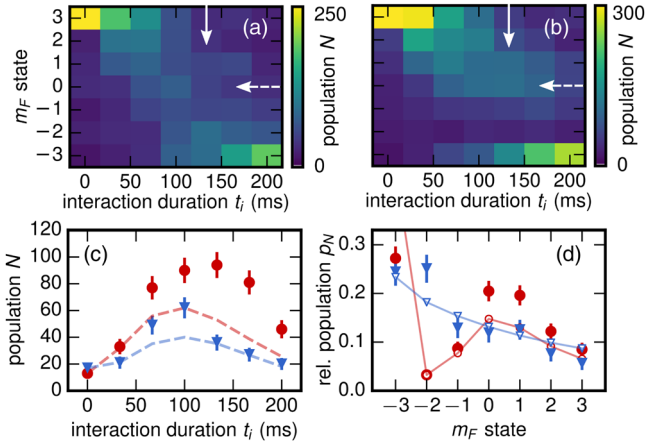

FIG. 2. Spin control in the Feshbach resonance regime. SE dynamics of Cs atoms (initially in $m_{F,\mathrm{Cs}} = 3$), immersed in a Rb bath of $m_{F,\mathrm{Rb}} = 0$. The color code indicates the total measured Cs population N for respective $m_{F,\mathrm{Cs}}$ states. (a) Measurement at $B = 440$ mG, showing uniform $m_{F,\mathrm{Cs}}$ evolution. SE occurs at rate $\approx\Gamma_{+1} = 26$ Hz for our density overlap of $\langle n\rangle = 2 \times 10^{12}$ cm^{-3}. (b) Measurement at $B = 220$ mG shows a metastable $m_{F,\mathrm{Cs}} = 0$ state, where the population freezes in the vicinity of the zero value of the SE scattering section of the $|-1, 0\rangle$ Feshbach resonance [compare Fig. 1(b)]. (c) Time evolution of the $m_{F,\mathrm{Cs}} = 0$ population [dashed arrow in (a),(b)] for B fields of (a) (triangle) and (b) (circles) compared to results of our coupled-channel model (dashed lines, no free parameters), demonstrating the emergence of a metastable state $m_{F,\mathrm{Cs}} = 0$ in the resonance regime (b). (d) $m_{F,\mathrm{Cs}}$ population for a given interaction time $t_i = 120$ ms [solid arrow in (a),(b)], showing enhanced population in $m_{F,\mathrm{Cs}} = 0$ and suppressed population in $m_{F,\mathrm{Cs}} = -2$. Open symbols show the same model as in (c), with solid lines guiding the eye. Atom counts in (a)–(c) result from the repetition of the experiment under the same conditions and error bars give statistical count uncertainties.

A very different picture emerges, when the spin evolution of Cs, initially in $m_{F,\mathrm{Cs}} = 3$, is recorded at a smaller magnetic field of 220 mG [see Fig. 2(b)]. Here, the population splits into two parts, one remaining in $m_{F,\mathrm{Cs}} = 0$, while another part is pumped to $m_{F,\mathrm{Cs}} = -3$. This emergence of a metastable $m_{F,\mathrm{Cs}}$ (here $m_{F,\mathrm{Cs}} = 0$) state is a direct hallmark of a magnetic Feshbach resonance in our system [regime *I* in Fig. 1(b)]: In the vicinity of Feshbach resonances in multiple scattering channels [compare Fig. 1(b)], SE cross section of the $|0, 0\rangle$ and $|-1, 0\rangle$ channels are suppressed for a wide range of collisional energies due to the zero value of scattering cross sections σ_1. At the same time, interaction in the $|-2, 0\rangle$ channel is strongly enhanced at the same B field, leading to a fast depopulation. Consequently, SE does not lead to a uniform pumping to the $m_{F,\mathrm{Cs}} = -3$ state (regime *I*). We include the thermal distribution of collision energies $p(E_{\mathrm{coll}})$ into our model (see [23]) and find excellent agreement with our measurements [see Figs. 2(c) and 2(d)].

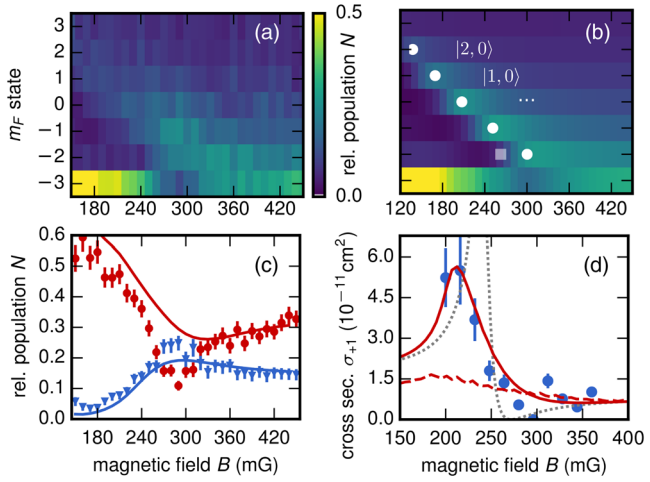

FIG. 3. Low-energy Feshbach spectroscopy. Spin population of Cs (initially in $m_{F,\mathrm{Cs}} = 3$) immersed in a Rb $m_{F,\mathrm{Rb}} = 0$ bath for $t_i = 100$ ms and various magnetic fields. (a) Metastable states, where the evolution towards the global energy minimum with $m_{F,\mathrm{Cs}} = -3$ is interrupted in multiple $|m_{F,\mathrm{Cs}}, m_{F,\mathrm{Rb}} = 0\rangle$ channels, indicating zero values of respective Feshbach resonances [marked in (b)]. High $m_F = -3$ population at low magnetic fields results from enhanced SE cross sections in all channels at low B fields and thermal broadening [see Fig. 1(b)]. (b) Coupled-channel scattering model corresponding to measurement in (a), including thermally distributed relative collision energies (no free parameters), which shifts the Feshbach zero value (white square) towards higher B fields (white circles). (c) Comparison of measurement (a) (data points) and our model (b) (solid lines) for two Cs states $m_{F,\mathrm{Cs}} = -3$ (red) and $m_{F,\mathrm{Cs}} = -1$ (blue), showing excellent agreement. (d) Direct measurement of the scattering cross section for $\Delta m_F = 1$ in the $|-2,0\rangle$ channel, by measuring $m_{F,\mathrm{Cs}}$ populations for two interaction times t_i (see [23]). Lines show the coupled-channel results for a fixed collision energy (gray), and temperature-broadened model for $T = 450$ nK (red, solid) and $T = 1.5$ μK (red, dashed).

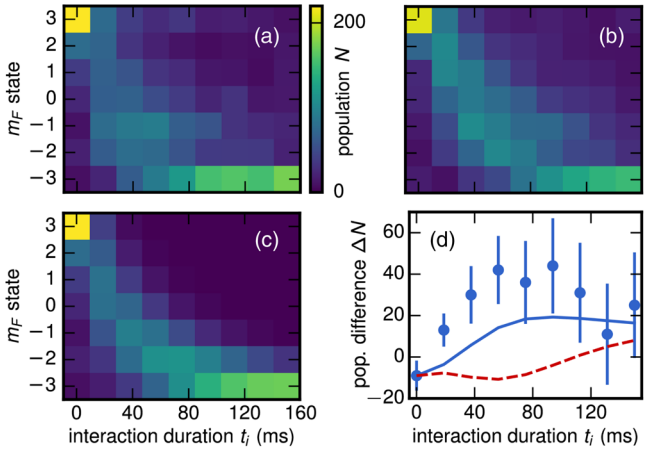

FIG. 4. SE measurement with $\Delta m_F = 2$. Spin evolution of Cs $m_{F,\mathrm{Cs}} = 3$ in Rb $m_{F,\mathrm{Rb}} = -1$ bath, measured for (a) $B = 50$ mG and (b) $B = 250$ mG. (c) Modeled evolution (no free parameters) for settings in (a). (d) Difference of low and high B-field evolution in $m_{F,\mathrm{Cs}} = -3$ state. Positive values mean faster evolution at low B-field values (data points). Solid lines give the expectation from our model, including $2\hbar$SE (blue, solid), and a model, where $2\hbar$ processes are excluded (red dashed), for comparison. Counts and errors, see Fig. 2.

In order to find resolution limitations, we probe the energy distance between the Feshbach resonances in subsequent channels. Therefore, we scan the magnetic field over the range of expected Feshbach resonances [see Fig. 3(a)] for a constant Cs-Rb interaction time. We find population enhancement in $m_{F,\mathrm{Cs}}$ states to emerge in all scattering channels, where we expect Feshbach resonances [see Fig. 3(c)], as discussed before. A clear distinction of individual resonances is only possible for narrowly distributed collision energies $p(E_{\mathrm{coll}})$ at ultralow temperatures. By contrast, if the thermal spread $\Delta E_{\mathrm{coll}} \approx \sqrt{3/2} k_B T$ strongly exceeds the width of the Feshbach resonance $\gamma \Delta B$ (γ is the magnetic moment of the Feshbach bound state, see [23]), the thermally averaged cross section does not show a minimum; thus it cannot be identified via a metastable Zeeman population. In fact, for $T = 450$ nK ($\Delta E_{\mathrm{coll}}/h = 9.4$ kHz) the occupation of metastable states is less pronounced for lower-lying Feshbach resonances, where the width of the Feshbach resonances is decreasing, e.g., 27 mG (9.5 kHz) for $|-2,0\rangle$ channel versus 10 mG (3.5 kHz) for $|2,0\rangle$ [see Fig. 3(a)]. The influence of thermal broadening on the resolution is shown in Fig. 3(d). Here, we compare a direct measurement of the SE cross section σ_1 in the collision channel $|-2,0\rangle$ with our finite-temperature model [23] and find excellent agreement. By contrast, already at a bath temperature of 1.5 μK ($\Delta E_{\mathrm{coll}}/h = 31$ kHz) thermal broadening impedes the resolution of individual Feshbach resonances, underlining the necessity to employ thermalized impurities at ultralow temperatures. Finally, we turn to the situation of a Rb bath in $m_{F,\mathrm{Rb}} = -1$, where SE processes in quanta of $2\hbar$ ($\Delta m_F = 2$) become significant for low magnetic fields ($B < 50$ mG). In order to distinguish $\Delta m_F = 2$ SE from $\Delta m_F = 1$ processes ($\sigma_1 \approx 10\sigma_2$), two data sets are taken at magnetic fields at 50 and 250 mG [see Figs. 4(a) and 4(b)], respectively. At these fields, SE rates for $\Delta m_F = 1$ processes are the same to a level of $\approx 1\%$, while σ_2 cross sections differ by a factor of 2. As a consequence, we expect a faster spin evolution for Cs at the lower magnetic field, driven by the influence of $\Delta m_F = 2$ SE. In our experiment, we realize the same bath conditions for both magnetic fields by iteratively changing the background field in the measurement throughout a total of 14×10^3 independent runs. We compare both SE series, calculating the population difference $N^{50\ \mathrm{mG}}_{m_{F,\mathrm{Cs}}} - N^{250\ \mathrm{mG}}_{m_{F,\mathrm{Cs}}}$. Thereby, we effectively exclude the influence of $\Delta m_F = 1$ and find a faster $m_{F,\mathrm{Cs}} = -3$ pumping for the lower magnetic field, as expected [see Fig. 4(d)]. The behavior is reproduced by the full rate model, including both $\Delta m_F = 1$ and $\Delta m_F = 2$ processes. By contrast, when excluding $\Delta m_F = 2$ from

our model, the difference in $m_{F,\mathrm{Cs}} = -3$ pumping is negligible and the measured faster population of $m_{F,\mathrm{Cs}} = -3$ at low magnetic field cannot be reproduced. We conclude that our observation reveals SE processes in quanta of $2\hbar$, driven by hyperfine interaction, only.

Controlling individual impurity-bath collisions at $h \times$ kHz energies has enabled the exploration of new SE regimes, with numerous future perspectives. Ultralow energies allow studying and controlling individual reaction processes with Zeeman-state resolution. Furthermore, the collision energy E_{coll} is tunable by accelerating Cs impurities in a species-specific transport lattice [18], allowing for high collision energies at ultralow temperatures. Finally, at even lower energies, endoergic SE with $\Delta m_F = -1$ becomes appreciable, turning the impurities' spin-state manifold into a local, highly sensitive probe of the bath's kinetic energy distribution. This might facilitate, for instance, the probing of quantum many-body relaxation by impurity immersion, when the bath has been driven out of equilibrium.

We thank Michael Hohmann and Axel Pelster for helpful discussions. This work was funded in the early stage by the European Union via ERC Starting grant "QuantumProbe" and in the final stage by Deutsche Forschungsgemeinschaft via Sonderforschungsbereich (SFB) SFB/TRR185. D. M. and F. S. acknowledge partial funding via SFB/TRR49, T. L. acknowledges funding by Carl Zeiss Stiftung, and F. S. acknowledges funding by the Studienstiftung des deutschen Volkes.

*widera@physik.uni-kl.de

[1] S. A. Moses, J. P. Covey, M. T. Miecnikowski, D. S. Jin, and J. Ye, Nat. Phys. **13**, 13 (2016).
[2] J. L. Bohn, A. M. Rey, and J. Ye, Science **357**, 1002 (2017).
[3] M. A. Baranov, M. Dalmonte, G. Pupillo, and P. Zoller, Chem. Rev. **112**, 5012 (2012).
[4] G. Quemener and P. S. Julienne, Chem. Rev. **112**, 4949 (2012).
[5] M. S. Safronova, D. Budker, D. DeMille, D. F. J. Kimball, A. Derevianko, and C. W. Clark, Rev. Mod. Phys. **90**, 025008 (2018).
[6] J. Weiner, V. S. Bagnato, S. Zilio, and P. S. Julienne, Rev. Mod. Phys. **71**, 1 (1999).
[7] F. H. J. Hall and S. Willitsch, Phys. Rev. Lett. **109**, 233202 (2012).
[8] J. Wolf, M. Deiß, A. Krükow, E. Tiemann, B. P. Ruzic, Y. Wang, J. P. D'Incao, P. S. Julienne, and J. H. Denschlag, Science **358**, 921 (2017).
[9] T. Sikorsky, Z. Meir, R. Ben-Shlomi, N. Akerman, and R. Ozeri, Nat. Commun. **9**, 920 (2018).
[10] L. R. Liu, J. D. Hood, Y. Yu, J. T. Zhang, N. R. Hutzler, T. Rosenband, and K.-K. Ni, Science **360**, 900 (2018).
[11] M. Schlagmüller, T. C. Liebisch, F. Engel, K. S. Kleinbach, F. Böttcher, U. Hermann, K. M. Westphal, A. Gaj, R. Löw, S. Hofferberth, T. Pfau, J. Pérez-Ríos, and C. H. Greene, Phys. Rev. X **6**, 031020 (2016).
[12] K. S. Kleinbach, F. Engel, T. Dieterle, R. Löw, T. Pfau, and F. Meinert, Phys. Rev. Lett. **120**, 193401 (2018).
[13] A. Bennett, K. Gibble, S. Kokkelmans, and J. M. Hutson, Phys. Rev. Lett. **119**, 113401 (2017).
[14] J. G. Danzl, M. J. Mark, E. Haller, M. Gustavsson, R. Hart, J. Aldegunde, J. M. Hutson, and H.-C. Nägerl, Nat. Phys. **6**, 265 (2010).
[15] S. Ospelkaus, K.-K. Ni, D. Wang, M. H. G. de Miranda, B. Neyenhuis, G. Quéméner, P. S. Julienne, J. L. Bohn, D. S. Jin, and J. Ye, Science **327**, 853 (2010).
[16] P. K. Molony, P. D. Gregory, Z. Ji, B. Lu, M. P. Köppinger, C. R. Le Sueur, C. L. Blackley, J. M. Hutson, and S. L. Cornish, Phys. Rev. Lett. **113**, 255301 (2014).
[17] D. Mayer, F. Schmidt, D. Adam, S. Haupt, J. Koch, T. Lausch, J. Nettersheim, Q. Bouton, and A. Widera, J. Phys. B **52**, 015301 (2019).
[18] F. Schmidt, D. Mayer, Q. Bouton, D. Adam, T. Lausch, N. Spethmann, and A. Widera, Phys. Rev. Lett. **121**, 130403 (2018).
[19] F. Schmidt, D. Mayer, M. Hohmann, T. Lausch, F. Kindermann, and A. Widera, Phys. Rev. A **93**, 022507 (2016).
[20] A. D. Lange, K. Pilch, A. Prantner, F. Ferlaino, B. Engeser, H.-C. Nägerl, R. Grimm, and C. Chin, Phys. Rev. A **79**, 013622 (2009).
[21] H. T. C. Stoof, J. M. V. A. Koelman, and B. J. Verhaar, Phys. Rev. B **38**, 4688 (1988).
[22] T. Takekoshi, M. Debatin, R. Rameshan, F. Ferlaino, R. Grimm, H.-C. Nägerl, C. R. Le Sueur, J. M. Hutson, P. S. Julienne, S. Kotochigova, and E. Tiemann, Phys. Rev. A **85**, 032506 (2012).
[23] See Supplemental Material at http://link.aps.org/supplemental/10.1103/PhysRevLett.122.013401 for details on experimental and data analysis procedures, which includes Refs. [24–31].
[24] T.-L. Ho, Phys. Rev. Lett. **81**, 742 (1998).
[25] T. Ohmi and K. Machida, J. Phys. Soc. Jpn. **67**, 1822 (1998).
[26] M. Mudrich, S. Kraft, K. Singer, R. Grimm, A. Mosk, and M. Weidemüller, Phys. Rev. Lett. **88**, 253001 (2002).
[27] J. M. Hutson, E. Tiesinga, and P. S. Julienne, Phys. Rev. A **78**, 052703 (2008).
[28] C. Chin, R. Grimm, P. Julienne, and E. Tiesinga, Rev. Mod. Phys. **82**, 1225 (2010).
[29] C. L. Blackley, P. S. Julienne, and J. M. Hutson, Phys. Rev. A **89**, 042701 (2014).
[30] M. Cannoni, Phys. Rev. D **89**, 103533 (2014).
[31] E. Tiesinga, B. J. Verhaar, and H. T. C. Stoof, Phys. Rev. A **47**, 4114 (1993).
[32] F. Dalfovo, S. Giorgini, L. P. Pitaevskii, and S. Stringari, Rev. Mod. Phys. **71**, 463 (1999).
[33] M. Hohmann, F. Kindermann, T. Lausch, D. Mayer, F. Schmidt, E. Lutz, and A. Widera, Phys. Rev. Lett. **118**, 263401 (2017).
[34] D. M. Stamper-Kurn and M. Ueda, Rev. Mod. Phys. **85**, 1191 (2013).
[35] S. D. Gensemer, R. B. Martin-Wells, A. W. Bennett, and K. Gibble, Phys. Rev. Lett. **109**, 263201 (2012).
[36] S. Hensler, J. Werner, A. Griesmaier, P. O. Schmidt, A. Görlitz, T. Pfau, S. Giovanazzi, and K. Rzazewski, Appl. Phys. B **77**, 765 (2003).